Vectorial On-Surface Synthesis of Polar 2D Polymer Crystals

*Takahiro Kojima, Karan Patel, Shunpei Nobusue, Ahmed Mahmoud, Cong Xie, Takahiro Nakae, Shigeki Kawai, Kazuhiro Fukami, and Hiroshi Sakaguchi**

The asymmetric introduction of functional groups into polymers is promising due to its potential to provide novel electronic and magnetic properties. Though traditional on-surface bottom-up synthesis has succeeded in creating various types of polymers, it struggles at realizing asymmetry due to the difficulty of stereoregular polymerization and the tendency for overall polarity cancellation during agglomeration. Here, enabled by the low halogen-contaminated metal surfaces provided by two-zone chemical vapor deposition, "compass" precursors possessing three independent bonding, edge, and dipole vectors undergo isotactic polymerization via the vectorial self-assembly of chiral precursor diradicals without the need for chiral catalysts required in conventional in-solution polymerization. The isotactic polymers exhibit polar 2D crystalline structures due to the hetero-edge CH–π interaction between the standing phenyl and butoxy group surpassing the homo-edge interactions of π–π and CH–CH. The developed vectorial on-surface synthetic technique not only paves the way to the realization of stereoregular control but also unlocks unprecedented crystal engineering.

1. Introduction

Asymmetric structures play crucial roles in producing particular properties and functionalities in various scopes of physics, chemistry, and biology.[1–4] For example, ferroelectrics require the noncentrosymmetric alignment of electric dipoles, and ferromagnetism needs spins to be coupled nominally in the same direction.[2–3] 1D carbon-based nanostructures have attracted a lot of attention because their electronic or magnetic properties can, in principle, be controlled by the introduction of functional groups.[5,6] Although on-surface synthetic techniques based on chemical reactions taking place on metal surfaces under ultrahigh vacuum (UHV) conditions have succeeded in creating various types of polymers, all those reported so far are limited to nonpolar structures.[7–11] To create the novel class of electronically asymmetric polymers, predicted to bear promising functionality for new applications,[1–4] brand new synthetic methods are required since conventional on-surface synthesis techniques suffer from the difficulties of stereoregular polymerization of the precursors and the polar interstrand order of the polymers. To overcome these challenges, we designed the compass precursors, which, due to their bonding and edge vectors, are capable of aligning their reaction intermediates in the same 2D vectorial direction that leads to isotactic polymers with the polar 2D crystalline structures under two-zone chemical vapor deposition (CVD) (**Figure 1**a).

2. Results and Discussion

Z-bar-linkage type precursors (molecules possessing two polyphenylene branches linked at hinge positions that look like the letter "z") were used in this study. The backbone of these precursors allows them to adopt various conformations due to its flexibility at the hinge position while simultaneously holding rigid polyphenylene branches. Our previous work found that two-zone CVD of the symmetric z-bar-linkage precursor 4″,5‴-dibromo-1,1′:4′,1″:2″,1‴:2‴,1⁗:4⁗,1⁗′-sexiphenyl resulted in the formation of homochiral polymers and their following conversion into cove-edged graphene nanoribbons (GNRs).[12] The key to the success of this process is believed to be the dynamic chirality of the precursor's diradical in which the achiral (C_{2h}) forms in the gas phase might be transformed into chiral (C_1) forms when deposited on the metal surface. In this study, 3-vectorial; C_s symmetry z-bar-linkage precursors with three vectors (dynamic chirality-driven bond (polymerization) vector, unidirectional intermolecular force-inducing edge vector

T. Kojima, K. Patel, S. Nobusue, A. Mahmoud, C. Xie, H. Sakaguchi
Institute of Advanced Energy
Kyoto University
Kyoto 611-0011, Japan
E-mail: sakaguchi@iae.kyoto-u.ac.jp
T. Nakae
Smart Materials and Devices Innovation Center
KRI Inc.
Kyoto 600-8813, Japan
S. Kawai
Research Center for Advanced Measurement and Characterization
National Institute for Materials Science
Ibaraki 305-0047, Japan
K. Fukami
Department of Materials Science and Engineering
Kyoto University
Kyoto 606-8501, Japan

The ORCID identification number(s) for the author(s) of this article can be found under https://doi.org/10.1002/admi.202300214

DOI: 10.1002/admi.202300214

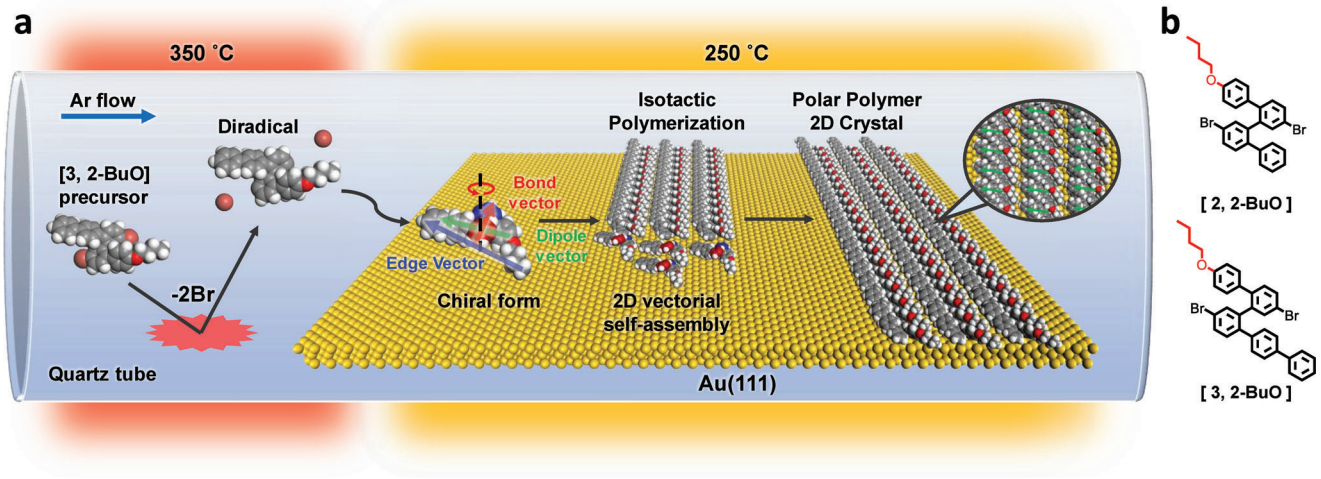

Figure 1. Concept illustration of the vectorial on-surface synthesis of polar 2D polymer crystals. a) Schematic representation of the polar 2D polymers synthesis process indicating the 3-vectorial precursor diradical formation and consequent polymerization via two-zone CVD. b) Illustrations of the chemical compounds utilized in this study.

and electronic asymmetry-inducing dipole vector) are designed to create polar polymers. The two strategies implemented in designing the asymmetric precursors are the length control of the polyphenylene branches and the introduction of the electronic asymmetry-inducing butoxy (abbreviated to –BuO) functional group. The n in the [n, m] notation refers to the number of benzene units in the z-bar-linkage precursor's aryl branch and the m refers to the number of benzene units in the modifier functional group branch. According to our strategy, two kinds of asymmetric precursors were synthesized: [2, 2-BuO] (4″,5‴-dibromo-4-butoxy-1,1″:2″,1‴:2‴,1⁗-quaterphenyl) and [3, 2-BuO] (4″,5‴-dibromo-4-butoxy-1,1″:2″,1‴:2‴,1⁗:4⁗,1⁗⁗-quinquephenyl) (Figure 1b).

The on-surface polymerization of [2, 2-BuO] and [3, 2-BuO] precursors was attempted using our two-zone CVD technique.[13] Two-zone CVD is based on the independent control of temperatures at precursor sublimation (T_{pre}), tube hot wall (T_{wall}) in zone 1, and Au(111) substrate (T_{sub}) in zone 2 to optimize the yield of products (Figure S1, Supporting Information). To identify the produced species, ex situ low-temperature scanning tunneling microscopy (LT-STM) measurements at 77 K under UHV conditions were conducted on samples transferred from the two-zone CVD apparatus. LT-STM images of two-zone chemical vapor deposited [2, 2-BuO] precursors on Au(111) at a T_{sub} of 250 °C reveal the formation of linear strands with dots at their edges (**Figure 2**a). The spacing of the dots along each strand's side is measured to be 0.74 nm (Figure 2b) and its width is found to be 1.72 nm (Figure 2c). These values are in good agreement with those based on the [2, 2-BuO] polymer structure shown in Figure 2d. By analyzing the magnified LT-STM images as shown in Figure 2e, two kinds of dot patterns—single dots depicted in green and unequally sized pairs of dots, referred to as "binary", marked red—are seen at the edges along the strands. Moreover, positions of the dots appearing at one side of the strands and those on opposite sides are found to be roughly 180° out of phase relative to each other. These results suggest that the binary dots correspond to the butoxyphenyl group, whereas the single dots are attributed to the edge phenyl groups (Figure 2d,e) supported by the STM simulation (Figure S2d, Supporting Information). According to the results of scanning tunneling spectroscopy (STS), the bandgap of [2, 2-BuO] is found to be 2.92 eV, as depicted in Figure 2f. This closely resembles the bandgap of poly-*p*-phenylene on Au(111), which is 3.23 eV.[14] The density functional theory (DFT) predicted the bandgap value of [2, 2-OBu] to be 2.86 eV, as seen in Figure S2a (Supporting Information). The simulated HOMO and LUMO energy levels are located at −0.58 and +2.28 eV, respectively, which are akin to those of [2, 2] without the butoxy group (Figure S2f , Supporting Information), which are −0.60 and +2.34 eV, correspondingly. Furthermore, the simulation of [2, 2-BuO] revealed the appearance of the HOMO+1 peak at −1.04 eV, indicating the contribution of the butoxy group. Next, we focus on the stereoregularity of the [2, 2-BuO] polymer. In general, polymer stereoregularity is categorized into three types: atactic, in which the asymmetric substituents are randomly arranged along the polymer backbone, alternatingly arranged in syndiotactic and unidirectionally arranged in the isotactic conformation (Figure 2g).[15] The LT-STM image shown in Figure 2e provides evidence that the polymer strands are atactic because the strand substituents appear to be joined in random orientations. Using a definition of m/(m + r), where m and r denote meso and racemo consecutive substituent ordering, respectively, as shown in Figure S2b (Supporting Information),[15] the overall isotacticity of [2, 2-BuO] polymers is assigned a value of 0.76 (Figure 2a).

LT-STM images of samples produced by two-zone CVD using [3, 2-BuO] precursors (Figure 2h) reveals that the dots' spacing is 0.74 nm along the strand (Figure 2i) similar to that of [2, 2-BuO], however, a larger unit width of 1.61 nm (Figure 2j) is observed (compared with [2, 2-BuO]'s value of 1.38 nm as shown in Figure 2e. These values are in good agreement with those based on the [3, 2-BuO] polymer chemical structure depicted in Figure 2k. Different from [2, 2-BuO] polymers, high-resolution LT-STM images of [3, 2-BuO] polymers clearly show that two kinds of dots exist exclusively at the opposite sides of the strands; binary dots represented in red appearing at one side

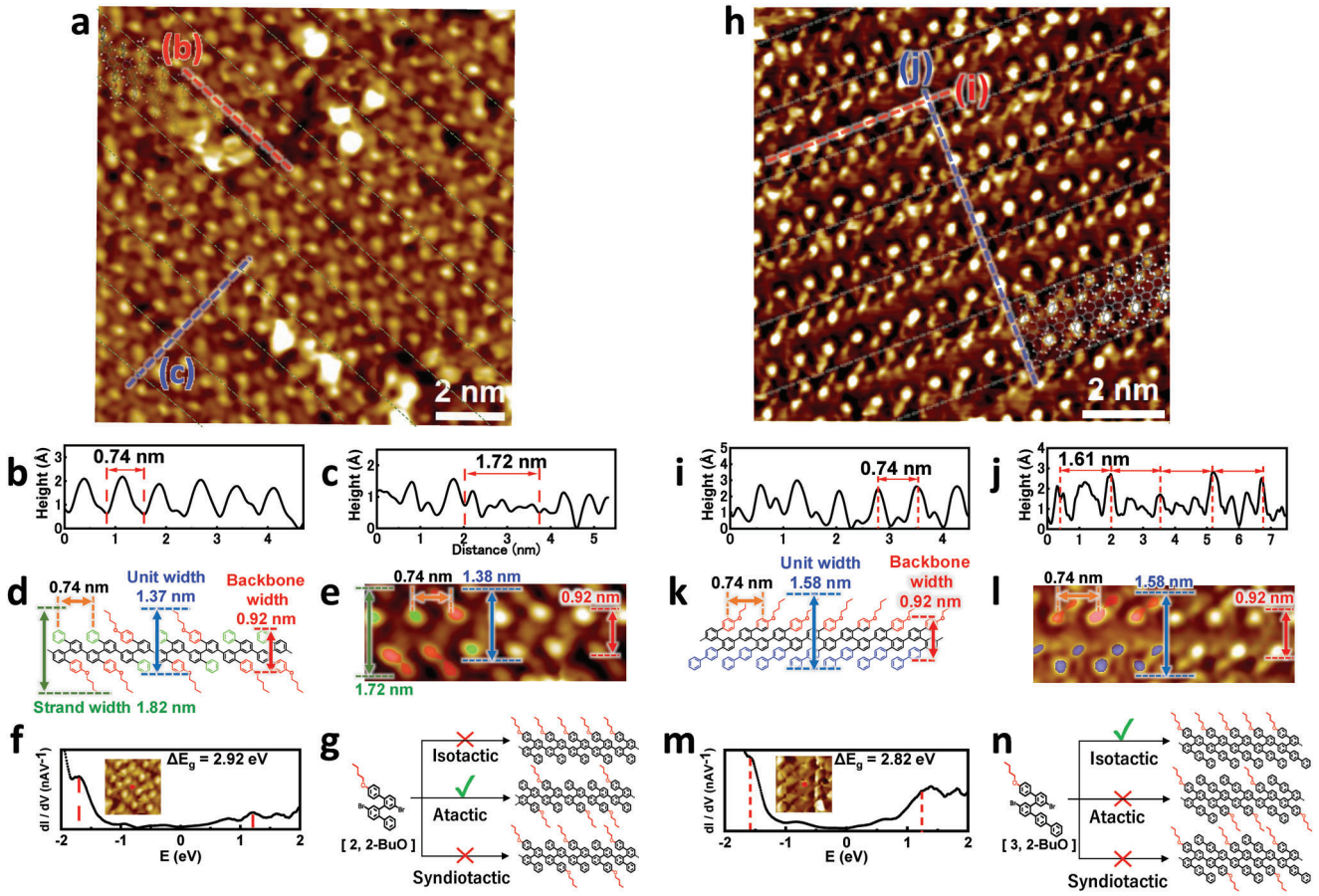

Figure 2. Stereoregular on-surface polymerization. a,h) LT-STM images and superimposed structures of [2, 2-BuO] (Bias voltage = −0.51 V, feedback current = 580 pA) and [3, 2-BuO] (−0.11 V, 580 pA) polymer strands. The white lines indicate strand boundaries, and the red and blue dotted lines mark the locations of the lateral and perpendicular topographic analysis paths, respectively. b,i) Topographic profiles of the red lines in (a,h). c,j) Topographic profiles of the blue lines in (a,h). d,k) Chemical structures of [2, 2-BuO] and [3, 2-BuO] polymers. e,l) Magnified LT-STM images of single [2, 2-BuO] (−0.75 V, 300 pA) and [3, 2-BuO] (−0.11 V, 580 pA) polymer strands. Green dots indicate edge phenyl groups, red binary dots indicate the butoxyphenyl groups and the twinned blue dots represent the biphenyl groups. f,m) Five times averaged STS profiles of [2, 2-BuO] and [3, 2-BuO] polymers. The insets indicate the STS measurement locations (red dots). The bandgap is estimated from the difference in potentials of the peaks indicated by red dotted lines. g,n) [2, 2-BuO] and [3, 2-BuO] polymer tacticity. [2, 2-BuO] precursors undergo atactic polymerization while [3, 2-BuO] precursors undergo isotactic polymerization.

of the strand, while similarly sized "twinned" dots depicted in blue are seen at the opposite side (Figure 2l) supported by the STM simulation (Figure S2e, Supporting Information). The dots are also roughly 180° out of phase. These results suggest that the binary dots correspond to the butoxyphenyl group, whereas the twinned dots are attributed to the biphenyl group at the edge of the other side (Figure 2k,l). Based on STS analysis, the products indicate a bandgap of 2.82 eV (Figure 2m) that is in good agreement with the DFT predicted value of 2.67 eV using the [3, 2-BuO] polymer model (Figure S2c, Supporting Information). These results imply that [3, 2-BuO] polymers were successfully formed. In stark contrast to [2, 2-BuO], analysis of the substrate's LT-STM images (Figure 2h,l) demonstrates that the isotacticity of [3, 2-BuO] polymers is unity, as the asymmetric substituents are arranged in a unidirectional manner, each along only one side of the polymer backbone (Figure 2n). This perfect isotacticity implies that the [3, 2-BuO] precursors spontaneously organize themselves unidirectionally—analogous to compass behavior—and then undergo radical coupling reactions to form covalent bonds.

We conducted a theoretical study with practical accuracy using quantum mechanics/molecular mechanics (QM/MM) simulations on the conformation of the precursor diradical on Au(111) as the polymer intermediate. Our aim is to understand the reason behind the isotactic polymerization in [3, 2-BuO] precursors compared to [2, 2-BuO] based on our previous report.[12] The conformation simulation on the [3, 2-BuO] and [2, 2-BuO] precursor diradicals generates eight chiral isomers in both precursor cases, categorized by two important factors: axis chirality (horizontal-axis chirality and vertical-axis chirality)[16] and enatiomerism (right-handed (*R*) and left-handed (*S*)) as shown in **Figure 3**a and Figure S3 (Supporting Information). Consequently, the eight isomers are named as a combination of the relative heights of the two hinge benzenes with regard to the Au(111) plane; if the height of one of the benzenes at the hinge is distant from the aforementioned plane, it is denoted as "u" (up), whereas if it is

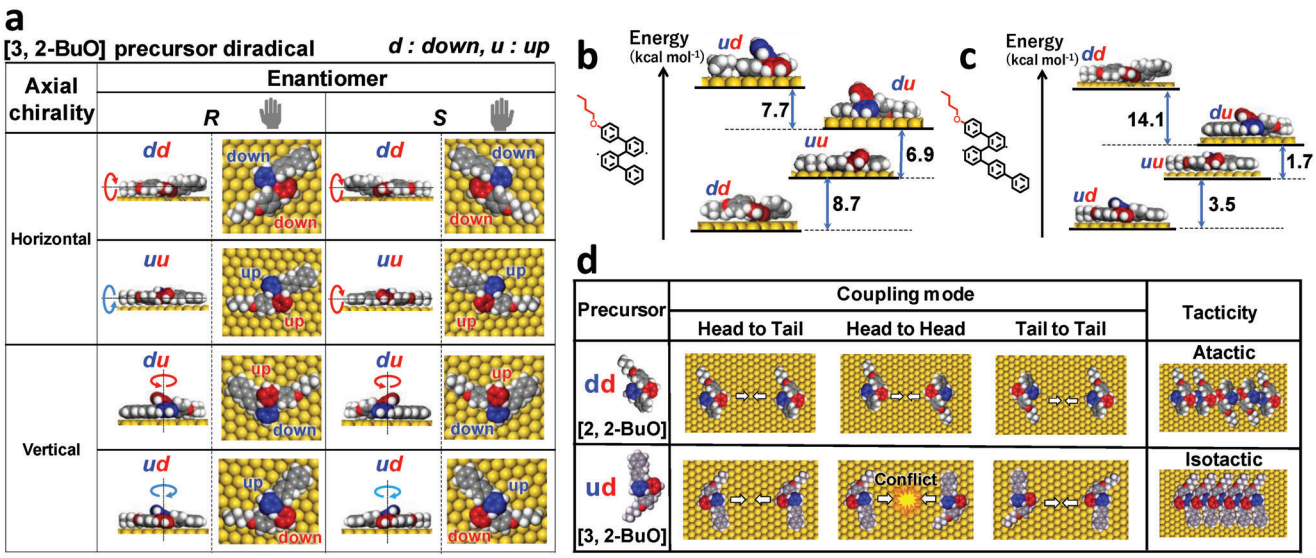

Figure 3. Mechanism of stereoregular on-surface polymerization. a) DFT predicted conformers of [3, 2-BuO] precursor diradicals on Au(111). b,c) Energy diagrams of the optimized [2, 2-BuO] and [3, 2-BuO] precursor diradical conformers on Au(111) highlighting the energy difference between them. d) [2, 2-BuO] and [3, 2-BuO] precursor diradicals' coupling modes.

located closer to character belongs the benzene of the aryl branch, which is denoted in blue, while the second letter belongs to the butoxy-group branch benzene that is denoted in red. Horizontal-axis chirality covers the [*uu*] and [*dd*] conformers that possess a chiral axis parallel to the Au(111) plane. On the other hand, the vertical-axis chirality group contains the [*ud*] and [*du*] conformers whose chiral axis is normal to the Au(111) plane. Additionally, the energy of all conformers was calculated by QM/MM to assess their thermodynamic stability. As a result, the [2, 2-BuO] precursor diradical favors the [*dd*] conformer on the Au(111) surface (Figure 3b) while the [3, 2-BuO] precursor diradical favors the [*ud*] conformer form (Figure 3c). Due to the difference in the metal-molecule interaction strength between the polar butoxy group and the nonpolar phenyl groups, the butoxy group branch is expected to adhere to the metal surface in contrast to the aryl branch benzenes that may levitate above the Au(111), resulting in the driving force behind the conformation change of the precursor diradicals.

The coupling reactions' modes were investigated using the previously generated chiral conformers to elucidate the stereoregular polymerization. Coupling reactions cover three modes: head-to-head, head-to-tail, and tail-to-tail.[17] Homo-coupling of the horizontally axial ([*dd*] + [*dd*]) [2, 2-BuO] precursor diradicals can adopt all three coupling modes due to the lack of steric hindrance between the coupling radicals, suggesting that atactic polymerization based on randomly oriented monomers should take place (Figure 3d). In sharp contrast, homo-coupling of the vertically axial ([*ud*]+[*ud*]) [3, 2-BuO] precursor diradicals exhibits no steric hindrance in the head-to-tail and tail-to-tail modes, while the head-to-head mode is disturbed (Figure 3d). Polymer growth can only proceed in the head-to-tail mode since the tail-to-tail mode causes strand termination, resulting in isotactic polymerization. These considerations support the experimental results, where the [2, 2-BuO] polymers are atactic (Figure 2g), while the [3, 2-BuO] polymers are isotactic (Figure 2n). According to previous in-solution studies, isotactic polymerization of asymmetric monomers (i.e., propylene) requires chiral catalysts such as Zeigler–Natta or metallocene that can coordinate and direct monomers for polymerization.[18,19] Our on-surface isotactic polymerization does not require chiral catalysts because the z-bar-linkage precursors spontaneously alter their shapes into chiral forms to unidirectionally align themselves.

2.1. In Sharp Contrast to the Purely Isotactic Polymers Obtained

Using two-zone CVD, LT-STM images of [3, 2-BuO] polymers prepared by the traditional UHV on-surface technique at 250 °C present mixtures of two kinds of polymers; those possessing chain-dot spacing of 0.75 nm (isotactic) and 1.48 nm in the other (syndiotactic; alternating sequential orientation) (**Figure 4**a–c).

It is well known that cleaved bromine atoms adhere to Au(111) under UHV on-surface synthetic techniques' conditions[20,21] that might alter the conformation of [3, 2-BuO] precursor diradicals on Au(111),[22] resulting in a change of coupling modes. Contrary to the UHV on-surface technique, two-zone CVD can provide large bromine-free Au(111) surfaces indicated by weak bromine XPS signals in the sample (Figure S4, Supporting Information). The reason behind the low bromine-Au(111) contamination might be the result of the separation of the molecular cleavage and polymer growth zones and the exhaust of the bromine atoms in the argon gas flow[12] in contrast to the UHV techniques where the halogen is trapped. This feature of two-zone CVD makes it a prerequisite for on-surface isotactic polymerization.

After thermal annealing at 400 °C, carbon monoxide-functionalized tip constant-height LT-STM images of in situ synthesized polymers using the UHV apparatus reveal the formation of GNRs of two kinds reflecting the tacticity of their parent polymers: isotactic and syndiotactic (Figure 4d,e; Figure S5,

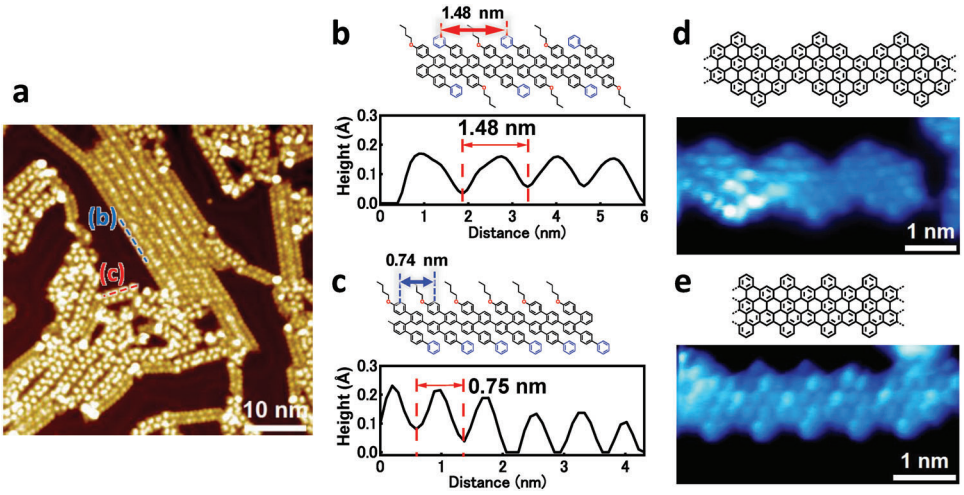

Figure 4. UHV on-surface synthesis of [3, 2-BuO] polymers. a) LT-STM (4K) image of [3, 2-BuO] polymer (−0.20 V, 10 pA) produced via the UHV deposition method at a substrate temperature of 250 °C. b,c) Topographic profiles of the lines in (a) demonstrating the different dot spacing between syndiotactic (1.48 nm) and isotactic (0.75 nm) polymer aggregates. The expected chemical structures are illustrated. d,e) Constant-height d*I*/d*V* images (1 mV, 10 pA) using a CO-functionalized tip of selected strands of UHV deposited [3, 2-BuO] polymers annealed at 400 °C and their expected chemical structures.

Supporting Information). The lack of functional groups in these GNRs provides evidence for their decomposition, proving that UHV synthesis is not suitable for creating asymmetric isotactic polymers.[23–25]

The simulated electrostatic potential mapping of [3, 2-BuO] polymers suggests that the per-monomer unit electric dipole is 1.87 Debye virtually perpendicular to the strand axis (**Figure 5**a). As the maximum observed length of strands measured in the LT-STM images of [3, 2-BuO] Polymers (Figure S6a, Supporting Information) is 35.3 nm (corresponding to 47 monomer units), strands are estimated to possess dipole moments of 88 Debye. To achieve thermodynamic stability, strands of polar polymers such as polyvinylidene difluoride (PVDF) tend to orient in an antiparallel manner to reduce the overall polarization.[26] On the contrary, the [3, 2-BuO] polymers' structure was discovered to belong to the unusual non-centrosymmetric 2D crystalline symmetry group in which every domain's strands' electric dipoles align unidirectionally virtually perpendicular to the strands (Figure 5b). In addition, the observed "inter-strands" uniform 1.61 nm spacing (Figure 2j) also supports the proposed polar 2D-crystal domains model. Consequently, the 2D polar polymer agglomerates can be categorized into the P_1 space group. It is well known that dielectric materials can be categorized according to the point groups of their crystals.[27] Among the 32 crystal symmetry point groups, 21 are non-centrosymmetric and can further belong to the special property classes of piezoelectric, pyroelectric and ferroelectric materials.[27] Thus, the 2D crystals of [3, 2-BuO] polymers are believed to be pyroelectric since their structure is non-centrosymmetric and polar. A theoretical study based on the inter-chain interaction energies of two molecular groups (aryl and alkyl) was conducted on [3, 2-BuO] polymers to identify the reason for the overall polar inter-chain arrangement of the [3, 2-BuO] polymers. Three modes of inter-chain interactions can be considered, CH-π interactions (Figure 5c), π–π (Figure 5d) and CH–CH interactions (Figure 5e).[28–30] The energy for the three interaction modes was calculated by DFT using the generalized gradient approximation of the Perdew–Burke–Ernzerhof (GGA-PBE) functional that accounts for the noncovalent molecular interactions without solid surfaces.[31] In this calculation, one strand's coordinates were fixed, and the second's was placed in close proximity to the fixed one and its location adjusted in small increments in the X and Y directions (Figure 5c). DFT energy calculations were performed at all secondary strand coordinates. Assigning the energy minimum value (CH-π, Figure 5f) to zero, the relative energy landscapes based on this model reveal the energy difference for the other two interaction modes' minimum values to be 39.92 kcal mol^{-1} for π–π (Figure 5g), and 66.40 kcal mol^{-1} for CH–CH (Figure 5h). The optimized strands' geometry at the minimum energy for the three modes is represented in Figure 5c–e. Among the three modes of interaction, the CH-π mode possesses the least energy, suggesting that the structure resulting from it—the polar crystalline structure—is the most energetically favorable. The theoretical study also estimates that the inter-strand distance in the optimized CH-π configuration is 1.61 nm (Figure 5c). In principle, π–π interactions are known to be stronger than CH-π interactions and CH–CH interactions in solutions.[28] However, the results we obtained deviate from the norm. The reason behind this phenomenon presumably originates from steric hindrance; narrow spaces resulting from the massive edge-phenyl groups hinder π–π inter-chain interaction by forbidding the approach of neighboring strands' phenyl groups (Figure 5d). As a result, [3, 2-BuO] polymers express the unusual CH-π chemical interaction rather than that of π–π or CH–CH.

3. Conclusion

To summarize, the alignment of polymer strands in their crystal domains is a result of two of the precursors' three vectors. The bond vector aligns the diradicals along the polymerization "latitude" based on the energetic stability of the precursors' chiral conformities. The asymmetry vector of the edge butoxy and

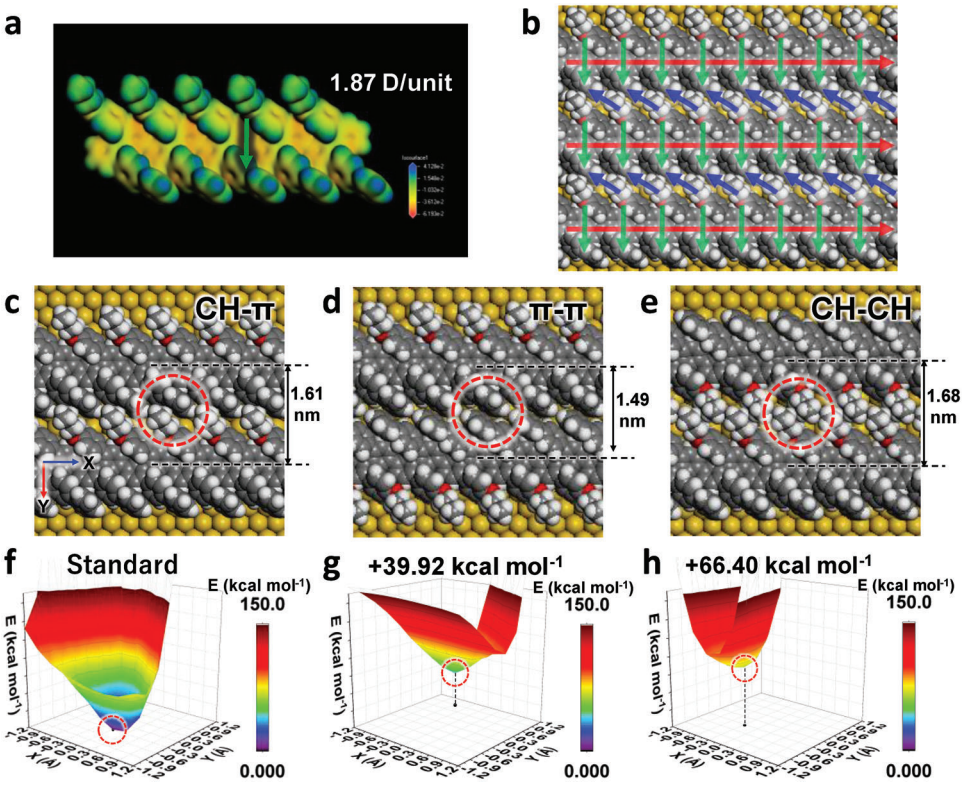

Figure 5. Polar 2D polymer crystals. a) Simulated electrostatic potential map of a [3, 2-BuO] 5mers. The green arrow indicates the per-monomer electric dipole of 1.87 Debye. b) Illustration of a polar 2D polymer crystal domain. The red, blue, and green arrows represent the bonding, edge, and dipole vectors, respectively. c–e) Illustrated interaction models of the optimized [3, 2-BuO] polymers indicating the optimum strand spacing for each interaction mode. The secondary polymer displacement axes are illustrated in (c). The red dotted circles indicate the typical interacted position. f–h) Contour maps of edge-group interaction energy as a function of *X* and *Y* displacement. The red dotted circles indicate the energy minima at the optimum inter-strand distances.

phenyl groups provides "longitudinal" inter-chain forces due to inter-strand edge group interaction, which we call "2D vectorial self-assembly." This process is capable of producing polar crystals (as shown in Figure 5b). These findings open up the possibility of creating polar 2D assemblies of 3-vectorial building blocks, which could lead to a new approach in polar crystal engineering.[32]

4. Experimental Section

STM Measurements: STM measurements except Figure 4 were performed under the constant-current mode with a commercially available UNISOKU low-temperature scanning tunneling microscopy system (USM-1100SA-2C) at 77 K. An electrochemically etched tungsten wire was used as the tip. Before conducting LT-STM and XPS measurements, all samples underwent pre-treatment in UHV conditions at 150 °C for 1 h to eliminate any adsorbed species. d*I*/d*V* spectra were acquired using the following conditions: $V_{sample} = -0.5$ V, $I = 200$ pA under the reduced feedback loop during voltage sweep. Additionally, STM measurements for Figure 4 were performed with commercially available Omicron low-temperature scanning tunneling microscopy and a homemade STM system, operating in ultra-high vacuum at temperatures below 5 K. High-resolution d*I*/d*V* imaging was performed with a CO-terminated tip, the differential conductance map was recorded by a digital lock-in amplifier with a modulation frequency of 510 Hz and an AC voltage of 10 mV. Obtained images were analyzed using the SPIP software.

Calculations: For the adsorption simulation of precursor on Au (111) surface, 100 different adsorption structures were calculated by the Monte Carlo method with a unit cell (46.24 × 40.05 × 49.72 Å) containing a three-layer gold substrate and a vacuum layer of 45 Å. The adsorption simulation was performed with the Adsorption Locator module based on the MM method, and COMPASS III was used for the force field. The precursor molecule was used as the initial structure. The obtained 100 structures were classified into four types, "*ud*", "*du*", "*dd*", and "*uu*", according to the difference in height between the two benzene rings at the molecule's hinge. One of each of the four structure types was optimized by the quantum mechanics/molecular mechanics (QM/MM) method (with the QMERA module).[33] The DMol3 module[34] and GGA-PBE exchange correlation functional were used to calculate the properties of the QM atoms and GULP was used to calculate the properties of the MM volumes employing the ReaxFF 6.0 force field.

Hydrogen-terminated GNR trimer models were used for the charge density and dipole estimation calculations. In the DMol3 module, a hybrid B3LYP functional with an all-electron core DN basis set was used. The grid interval was set to 0.25 Å, the orbital cutoff distance was set to 3 Å and the multipolar expansion was set to hexadecapole.

Regarding polymer inter-chain interaction energy, a unit cell (7.40 × 80.00 × 30.00 Å) was prepared, and two GNR strands were placed. Fine structural optimization calculation was performed by CASTEP module. DFT structural optimization and STM calculations, the Perdew–Burke–Ernzerhof generalized-gradient approximation (GGA-PBE)[35] was used as the exchange correlation functional employing on-the-fly-generated (OTFG) Ultrasoft pseudopotentials. The energy landscapes were constructed from the energy calculations performed at

each GNR strand coordinate. Inter-strand distance was set as the defined position of *X* and *Y*.

Supporting Information

Supporting Information is available from the Wiley Online Library or from the author.

Acknowledgements

This study was supported by KAKENHI Program No. 22H01891 (H.S.), 21K05038 (S.N.), and 22H00285(S.K.), the Japan Society for the Promotion of Science, Japan; Zero-Emission Energy Research (ZE2022B-07), IAE, Kyoto University (K.F.). A.M. thanks the Japanese Government (MEXT) for their generous scholarship. K.P thanks the MEXT-SGU for the scholarship.

Conflict of Interest

The authors declare no conflict of interest.

Data Availability Statement

The data that support the findings of this study are available in the Supporting Information of this article.

Keywords

polar 2D polymer crystals, stereoregular polymerization, vectorial on-surface synthesis

Received: March 13, 2023
Revised: April 28, 2023
Published online: June 16, 2023

[1] S. M. Morrow, A. J. Bissette, S. P. Fletcher, *Nat. Nanotechnol.* **2017**, *12*, 410.
[2] A. S. Tayi, A. Kaeser, M. Matsumoto, T. Aida, S. I. Stupp, *Nat. Chem.* **2015**, *7*, 281.
[3] J. S. Miller, *Mater. Today* **2014**, *17*, 224.
[4] N. Kirova, S. Brazovskii, *Synth. Met.* **2016**, *216*, 11.
[5] S. J. Higgins, *Chem. Soc. Rev.* **1997**, *26*, 247.
[6] A. Rajca, J. Wongsriratanakul, S. Rajca, *Science* **2001**, *294*, 1503.
[7] L. Grill, S. Hecht, *Nat. Chem.* **2020**, *12*, 115.
[8] S. Clair, D. G. de Oteyza, *Chem. Rev.* **2019**, *119*, 4717.
[9] Q. Shen, H.-Y. Gao, H. Fuchs, *Nano Today* **2017**, *13*, 77.
[10] L. Liu, X. Miao, T. Shi, X. Liu, H.-L. Yip, W. Deng, Y. Cao, *Nanoscale* **2020**, *12*, 18096.
[11] M. Di Giovannantonio, K. Eimre, A. V. Yakutovich, Q. Chen, S. Mishra, J. I. Urgel, C. A. Pignedoli, P. Ruffieux, K. Müllen, A. Narita, R. Fasel, *J. Am. Chem. Soc.* **2019**, *141*, 12346.
[12] H. Sakaguchi, S. Song, T. Kojima, T. Nakae, *Nat. Chem.* **2017**, *9*, 57.
[13] H. Sakaguchi, Y. Kawagoe, Y. Hirano, T. Iruka, M. Yano, T. Nakae, *Adv. Mater.* **2014**, *26*, 4134.
[14] N. M-Díez, A. G-Lekue, E. C-Sanromà, J. Li, M. Corso, L. Colazzo, F. Sedona, D. S-Portal, J. I. Pascual, D. G. de Oteyza, *ACS Nano* **2017**, *11*, 11661.
[15] G. M. Miyake, E. Y.-X. Chen, *Polym. Chem.* **2011**, *2*, 2462.
[16] G. Bringmann, A. J. Price Mortimer, P. A. Keller, M. J. Gresser, J. Garner, M. Breuning, *Angew. Chem., Int. Ed.* **2005**, *44*, 5384.
[17] T. A. Chen, R. D. Rieke, *J. Am. Chem. Soc.* **1992**, *114*, 10087.
[18] A. J. Teator, T. P. Varner, P. C. Knutson, C. C. Sorensen, F. A. Leibfarth, *ACS Macro Lett.* **2020**, *9*, 1638.
[19] A. J. Teator, F. A. Leibfarth, *Science* **2019**, *363*, 1439.
[20] C. Moreno, M. Panighel, M. Vilas-Varela, G. Sauthier, M. Tenorio, G. Ceballos, D. Peña, A. Mugarza, *Chem. Mater.* **2019**, *31*, 331.
[21] K. Sun, T. Nishiuchi, K. Sahara, T. Kubo, A. S. Foster, S. Kawai, *J. Phys. Chem. C* **2020**, *124*, 19675.
[22] R. Zuzak, A. Jančařík, A. Gourdon, M. Szymonski, S. Godlewski, *ACS Nano* **2020**, *14*, 13316.
[23] M. Panighel, S. Quiroga, P. Brandimarte, C. Moreno, A. Garcia-Lekue, M. Vilas-Varela, D. Rey, G. Sauthier, G. Ceballos, D. Peña, A. Mugarza, *ACS Nano* **2020**, *14*, 11120.
[24] H. Hayashi, J. Yamaguchi, H. Jippo, R. Hayashi, N. Aratani, M. Ohfuchi, S. Sato, H. Yamada, *ACS Nano* **2017**, *11*, 6204.
[25] E. Carbonell-Sanromà, J. Hieulle, M. Vilas-Varela, P. Brandimarte, M. Iraola, A. Barragán, J. Li, M. Abadia, M. Corso, D. Sánchez-Portal, D. Peña, J. I. Pascual, *ACS Nano* **2017**, *11*, 7355.
[26] Y.-J. Yu, A. J. H. McGaughey, *J. Chem. Phys.* **2016**, *144*, 014901.
[27] P.-P. Shi, Y.-Y. Tang, P.-F. Li, W.-Q. Liao, Z.-X. Wang, Q. Ye, R.-G. Xiong, *Chem. Soc. Rev.* **2016**, *45*, 3811.
[28] P. Yu, Y. Zhen, H. Dong, W. Hu, *Chem* **2019**, *5*, 2814.
[29] M. J. Plevin, D. L. Bryce, J. Boisbouvier, *Nat. Chem.* **2010**, *2*, 466.
[30] S. E. Wheeler, J. W. G. Bloom, *J. Phys. Chem. A* **2014**, *118*, 6133.
[31] F. Tran, R. Laskowski, P. Blaha, K. Schwarz, *Phys. Rev. B* **2007**, *75*, 115131.
[32] M. D. Hollingsworth, *Science* **2002**, *295*, 2410.
[33] P. Sherwood, A. H. de Vries, M. F. Guest, G. Schreckenbach, C. R. A. Catlow, S. A. French, A. A. Sokol, S. T. Bromley, W. Thiel, A. J. Turner, S. Billeter, F. Terstegen, S. Thiel, J. Kendrick, S. C. Rogers, J. Casci, M. Watson, F. King, E. Karlsen, M. Sjøvoll, A. Fahmi, A. Schäfer, C. Lennartz, *J. Mol. Struct.: THEOCHEM* **2003**, *632*, 1.
[34] B. Delley, *J. Chem. Phys.* **2000**, *113*, 7756.
[35] J. P. Perdew, K. Burke, M. Ernzerhof, *Phys. Rev. Lett.* **1996**, *77*, 3865.